

Faraday waves on a nematic liquid crystal, and its coupling with Marangoni convection about the thermal phase transition

O. Vázquez-Rodríguez^{1,*} and M. Hernández-Contreras²

¹*Facultad de Ciencias en Física y Matemáticas Universidad Autónoma de Chiapas, 29050 Tuxtla Gutierrez, Chiapas, México*

²*Departamento de Física Centro de Investigación y Estudios Avanzados del Instituto Politécnico Nacional Apartado Postal 14-740, 07360 México DF, México*



(Received 12 July 2023; accepted 17 October 2023; published 22 November 2023)

Using a linear hydrodynamic theory, we demonstrate that Faraday waves occur in liquid crystalline fluids. The use of already experimentally known material parameters of a *N*-(4-methoxybenzylidene)-4-butylaniline liquid crystal allows us to confirm and realize the predictions of this theory. It provides the critical wave number and necessary driving acceleration at instability wave onset. Additionally, these observables experience an abrupt change originated by Marangoni convection due to the temperature gradient at the isotropic-nematic phase transition temperature. Correspondingly, the Marangoni number versus temperature also shows a sharp change in the transition temperature.

DOI: [10.1103/PhysRevE.108.054703](https://doi.org/10.1103/PhysRevE.108.054703)

I. INTRODUCTION

Faraday waves arise at interfaces of fluids with air in a vessel that holds it and performs vertical motion [1,2]. It manifests in Newtonian [2–4] and complex fluids [5–16] as stationary symmetric patterns. This so-called parametric wave appears in experiments that include ferrofluids [6–8], electrolytes [3], polymeric [9–12], and micellar solutions [13–15]. There is no experimental observation of the Faraday instability on thermotropic liquid crystals. A theoretical prediction of its existence in liquid crystalline fluids of Smectic A type is found in Ref. [17]. Reference [13] provides a comprehensive experiment on filamentous fd virus suspension, which describes a Faraday wave in lyotropic liquid crystals during an isotropic-nematic phase change due to nematogen density variation at the interface. Reference [18] made a theoretical prediction on the effect of an isotropic-nematic phase change on the Faraday instability due to a temperature gradient. To our knowledge, there are no other reports on the study of this instability in liquid crystals. Liquid crystalline fluids present other interesting dynamical instabilities phenomena. One of these is Marangoni flow driven by surface tension variations. Since surface tension depends on temperature and chemical composition at the interface of a fluid, Marangoni flow may originate from gradients on both these thermodynamic variables. Those gradients produce Marangoni stresses at the interface. Therefore, there are viscous stresses due to fluid motion to counterbalance it. Marangoni flows induced by the temperature gradient of surface tension are called thermocapillary flows. In contrast, chemical composition gradients upon temperature change lead to Rayleigh-Benard convection (thermal volume buoyancy-driven convection). However,

Marangoni convection on thin liquid films is dominant over the Rayleigh-Benard convection owing to the predominance of thermocapillary forces at the interface over buoyancy volumetric effects [19]. The first experimental investigation of Marangoni flow in a quiescence droplet of nematic liquid crystal (NLC) deposited on a glass substrate revealed capillary waves due to surface viscosity originating from the Marangoni instability [20]. More recently, Rayleigh-Benard convection under magnetic fields on homeotropic NLC was researched experimentally in Ref. [21] for an NLC layer heated from below. Meanwhile, experiments on a layer of thermally equilibrated NLC with an exposed surface to air when heated from the air side with a laser beam develop Marangoni flow [22]. In this case, there is a mass transfer from the area of incident radiation radially outwards. In these experiments [22], the measured observables are the lateral in-plane hydrodynamic velocity at the nematic interface and the height of the interface deformation as a function of laser intensity. In Ref. [23], Choi and Takezoe exposed the free surface of an NLC film to laser light heating and observed circular flow formation triggered by Marangoni flow. Similar experiments by Shvetsov *et al.* [24] revealed light-induced umbilical defects on the free surface of NLC due to temperature gradient. They also found that absorption of light changes the nematic director field. Other experimental works by Roh *et al.* [25] showed that the presence of surfactants at the interface may change the orientation of the nematic director. They conducted experiments to understand the effects of a fluid flow at the interface of an aqueous solvent with solute surfactants in solution and a NLC to reorient the director parameter of NLC. Thus, this study identified the timescales at which surfactant concentration variation at the interface (a sign of Marangoni stresses) reaches a steady state through the orientation of the easy axis of the NLC at an isothermal condition. Reference [26] studied the Marangoni effect on the hydrodynamic flow velocity experimentally near the isotropic-nematic phase transition of an NLC. They found that the velocity flow direction depends on

*Author to whom correspondence should be addressed: oscar.rodriguez@unach.mx

the material coating the cell substrate that holds the nematic layer. They concluded that the flow direction gets reversed in the nematic phase compared to the isotropic phase. From the practical viewpoint, the Marangoni instability may make its use in inkjet printing patterns of liquid crystalline polymers feasible [27]. The Marangoni flow has also been comprehensively studied theoretically by Rey [28–30] for models of interfaces between isotropic surfactant solutions and NLCs with homeotropic boundary conditions and when subjected to temperature gradients [31]. The application of this theory to study the onset of thermocapillary and elongational waves induced by thermal fluctuations at the interface containing insoluble surfactants was performed by Ref. [32]. On the other hand, Popa-Nita and Oswald [33] developed a completely different theoretical approach based on the Landau-de Gennes free energy method to describe the capillary waves originating from thermal fluctuations at the interface of a ternary mixture of liquid crystal, colloid, and impurities. They considered two boundary conditions for the nematic director, homeotropic or variable orientation, to predict the dispersion relation of the thermal waves. Their results qualitatively confirmed Germano and Schmid's [34] molecular dynamics simulations on the thermal waves at the interface of isotropic nematics of a model of bulk ellipsoids with pairwise interaction of the Weeks-Chandler-Andersen type. References [35] and [36], respectively, are theoretical studies of Marangoni and Rayleigh-Benard, convection on homeotropic NLCs using a model of Gaussian light absorption at the nematic free surface. Finally, Refs. [37–41] make the theoretical prediction of different pattern formations at interfaces of NLC due to temperature gradient. Unlike all these studies of instability phenomena described above, only two theoretical calculations [17,18] and one experiment [13] reported the study of the Faraday instability in liquid crystalline fluids.

The present paper will study the Marangoni effect on the Faraday instability on nematic liquids. For isotropic fluids, previous studies of Faraday ripples in noncrystalline fluids by other authors [42,43] considered a rise in temperature without fluids experiencing a thermal phase transition. Such a temperature variation leads to particle flow at the interface (Marangoni effect). Investigation of Marangoni flow in isotropic fluids goes back to the '70s [42–45]. However, experiments and theoretical studies of the Faraday and Marangoni instabilities on liquid crystalline fluids still need to be included. This paper reports our modeling of the Faraday instability of a thermotropic NLC that experiences a thermal phase transition to an isotropic state for a realistic *N*-(4-methoxybenzylidene)-4-butylaniline (MBBA) nematic. The materials parameters of MBBA, surface tension, Leslie viscosities, and heat transport coefficients are well-known observables during its change from the nematic to its isotropic phase as a function of temperature [20,46,47]. Therefore, our modeling of this liquid crystal with the linear theory of Kumar and Tuckerman [48] does not contain free parameters. On the other hand, this linear theory has found excellent agreement with experiments on predicting the onset of Faraday waves in electrolytes [3], complex fluids [10,49], and computer simulations [50].

In our model of NLC with a free surface described in Sec. II, we consider the liquid crystal director to be in the same

direction as an applied external magnetic field and parallel to the liquid crystal air interface. Therefore, the nematic director never changes orientation when this system is under a temperature gradient. Consequently, the more general Q-tensor theory (which accurately considers the director's orientation) is unnecessary to describe this system's hydrodynamics. A second reason is that the Leslie-Ericksen theory we use in this paper explains quantitatively the measured observables in the experiments of Refs. [22,46]. Thus, in Sec. II we adapt the linear theory [46,48] to thermotropic liquid crystals. Here, we include the heat diffusion equation for the temperature variation that considers heat transfer normal to the interface in a typical experimental setup. This way, the Marangoni effect appears in the linear hydrodynamic theory. Sections III and IV refer to two crucial magnetic field configurations. Section V refers to our predictions on the necessary critical acceleration of the vessel for the onset of the instability and its corresponding wave number. During the phase transition, Marangoni effects manifest on both parameters, which experience a significant change for larger temperature gradients. We determine typical frequencies of oscillations and fluid depth effects on both critical parameters during the thermal phase transition. At the onset, the primary frequency is half the driving excitation one. We end Sec. VI with a conclusion.

II. PHYSICAL FORMULATION OF THE PROBLEM. CASE OF APPLIED MAGNETIC FIELD PARALLEL TO THE WAVE VECTOR ORIENTED ALONG THE x AXIS. NEMATIC DIRECTOR PARALLEL TO INTERFACE

In this section, we describe the hydrodynamic equation and its boundary conditions for a NLC layer with a free surface in contact with air. The equilibrium fluid under gravity follows an applied external vertical acceleration. Additionally, this system experiences a temperature gradient which induces a variation in the nematic surface tension with temperature. Therefore, the elastic in-plane elongational deformation of the interface appears as a Marangoni effect. Such an effect leads to the balance of tangential forces in both the interface and the vertical direction. A flat equilibrium interface of infinite lateral extension resides at $z = 0$, and a slab of nematic fluid occupies the space $-L \leq z \leq 0$. Above the free surface $z > 0$, there is air. At the interface reside mobile nematogens with their average orientation given by the nematic order parameter remaining firmly clamped in the direction of the external magnetic field. For this reason, there are no orientational fluctuations of the nematic director. The vessel with nematic liquid is under vertical acceleration $g(t) = g - a \cos(\omega t)$, where g is the gravitational acceleration. The reference frame moves with the container of fluid, where a is the external driving acceleration, and the oscillation frequency is ω . A static external magnetic field $\mathbf{H} = B\mu_0^{-1}\hat{\mathbf{e}}_x$ orients the director \mathbf{n} of the nematogens in the $\hat{\mathbf{e}}_x$ direction. $\mu_0 = 4\pi \times 10^{-7} \text{ N/A}^2$ is the permeability of free space. B is the magnetic induction. Due to symmetry in the spatial directions $\hat{\mathbf{e}}_x$ and $\hat{\mathbf{e}}_y$, we may assume the surface wave propagates in the $\hat{\mathbf{e}}_x$ direction with wave vector \mathbf{k} , thus coordinate y is ignored. A constitutive equation for the viscous stress tensor [46,47] relates the hydrodynamic velocity of the nematic liquid \mathbf{v} with its bulk shear viscosities η_2 , η_1 , and η' [47], through

$$\boldsymbol{\sigma}' = \eta' \mathbf{n}(\mathbf{n} \cdot \mathbf{E} \cdot \mathbf{n})\mathbf{n} + 2\eta_2 \mathbf{E} + 2(\eta_1 - \eta_2)[(\mathbf{nn} \cdot \mathbf{E}) + (\mathbf{nn} \cdot \mathbf{E})^T]. \quad (1)$$

The viscosities η_1, η_2, η' were measured in Ref. [46] for MBBA and their interpolations as a function of temperature. In Eq. (1), the unit vector director of the nematic molecules is given by $\mathbf{n} = (1, 0, 0) = \hat{\mathbf{e}}_x$. $\mathbf{E} = [(\nabla\mathbf{v}) + (\nabla\mathbf{v})^T]/2$ is the symmetric rate of strain tensor for linear and shear strain deformation without rigid body rotations. T stands for transpose. The velocity satisfies the linearized Navier-Stokes equation [46],

$$\rho \frac{\partial \mathbf{v}}{\partial t} = \nabla \cdot \boldsymbol{\sigma}, \quad (2)$$

where the total force per unit area acting on a fluid element is $\boldsymbol{\sigma} = -p\mathbf{I} - \boldsymbol{\sigma}' + \boldsymbol{\sigma}'' + z\rho g(t)\hat{\mathbf{e}}_z\hat{\mathbf{e}}_z$, with $\hat{\mathbf{e}}_z$ the unit vector along the z axis and $(\mathbf{I})_{\beta,\delta} = 1$ if $\beta = \delta$ and 0 otherwise. p is the hydrostatic fluid pressure, with ρ being the density. The solution of Eq. (2) supplemented with appropriate boundary conditions yields the components v_z and v_x of the velocity of deformation of the free surface on the nematic liquid. The elastic deformation of the interface occurs in the perpendicular and transversal in-plane directions. The elastic parameters associated with it are the surface tension γ and the in-plane longitudinal elastic constant ϵ for in-plane deformations. Their relationship occurs through the stress tensor $\boldsymbol{\sigma}'$, whose components provide the boundary conditions specified below. The normal deformation of the interface produces its elevation $\zeta(x, t)$. Such a normal stress jump across the nematic interface does not contribute to the in-plane longitudinal Marangoni stress and consequently to ϵ . Thus, tangential surface stresses are balanced by the viscous stresses of the fluid motion given by $\boldsymbol{\sigma}'$. To specify the notation in this paper, note that ϵ appears in the literature in two different but equivalent ways; one form is $\epsilon = S(\partial\gamma/\partial S)_T$ with S the local surface [51,52], T is the temperature. In contrast, the second way is $\epsilon = -\Gamma_0(\partial\gamma/\partial\Gamma)_T$ with Γ the in-plane spatially inhomogeneous concentration of insoluble molecules (nematogens) and Γ_0 its homogenous equilibrium value. Molecules are nematogens at the interface, whose number is constant but, at instability, get inhomogeneously distributed. They are insoluble and mobile at the interface. According to the chain rule, $\epsilon = S(\partial S/\partial\Gamma)^{-1}(\partial\gamma/\partial\Gamma)$, where $\Gamma = c_0/S$ with c_0 the proportionality constant, whose units can be molecules' moles per area or moles per length. Therefore, the surface S can be an effective area per mole or per molecule. Thus, $\partial S/\partial\Gamma = -c_0\Gamma^{-2}$, and from the above relation yields $\epsilon = -\Gamma_0(\partial\gamma/\partial\Gamma)_T$.

Because the liquid is kept under a vertical temperature gradient that produces a Marangoni instability [42], the temperature variations in the liquid are described by the linearized heat diffusion equation:

$$\partial_t T = Av_z + \alpha\nabla^2 T. \quad (3)$$

T is the local temperature variation concerning a reference state defined by $T_0 = Az + T_{00}$, with T_{00} an arbitrarily fixed temperature. The vertical gradient temperature per unit length A varies for each experimental temperature while keeping a fixed fluid thickness. It is $A < 0$ [53] for heating from the air side towards the bulk fluid [42]. Its value follows from the conditions at the bottom $z = -L$ where $T_0 = 273.15$ K and at the interface $z = 0$, where $T_0 = T_{\text{exp}}$ is the input experimental temperature. Thus, $T_{00} = T_{\text{exp}}$ from which

$A = -(T_{00} - 273.15)/L$ [43]. α is the anisotropic thermal diffusivity. Its value for the nematic MBBA is in Ref. [20], and it turns out to be larger along the long molecular axis than its normal value. It is negligibly small on the order of 10^{-7} m²/s. Therefore, its value does not contribute to the Faraday wave appreciably. For frequencies much less than the first sound frequency of the liquid, the incompressibility condition holds:

$$\nabla \cdot \mathbf{v} = 0. \quad (4)$$

The conservation equations of momentum Eq. (2), energy Eq. (3), and mass Eq. (4) are subjected to the boundary conditions at $z = -L$ of no slip,

$$\mathbf{v} = \mathbf{0}, \quad (5)$$

and no penetration:

$$\partial_z v_z = 0. \quad (6)$$

At the interface $z = 0$, the boundary conditions are the total normal and tangential stresses (forces per unit area) which satisfy the balance equations

$$\begin{aligned} \sigma_{zz} &= 0, \\ \sigma_{xz} &= 0, \\ \sigma_{yz} &= 0. \end{aligned} \quad (7)$$

However, the normal restoring surface (s) force f_z^s , also termed the Laplace term, is the mean surface tension at the given temperature $\gamma(T, \Gamma)$ [42]:

$$\sigma_{zz}^r = f_z^s = \gamma(T, \Gamma)\partial_x^2 \zeta(x). \quad (8)$$

ζ is the normal displacement of the interface from its equilibrium position. Additionally, the interface experiences elastic deformations arising from tangential shear and dilational surface viscosities [43]. The tangential surface (s) forces per unit area of dilational elasticity are [42]

$$\begin{aligned} \sigma_{xz}^r &= f_x^s = \partial_x \gamma(T, \Gamma), \\ \sigma_{yz}^r &= 0. \end{aligned} \quad (9)$$

The kinematic conditions are as follows because the displacement ζ is small compared with the wavelength:

$$\begin{aligned} \partial_t \zeta &= v_z, \quad \text{at } z = 0 \\ \partial_t \xi &= v_x, \end{aligned} \quad (10)$$

where ξ is the in-plane interface deformation.

To take into account the temperature and nematogen concentration gradients (spatial inhomogeneity) at the interface leading to Marangoni flow, we assume, as in Refs. [42,45], that γ is a linear function of temperature and molecule concentration,

$$\gamma(T, \Gamma) = \gamma_0 - \gamma_1(T - T_r) - \gamma_2(\Gamma - \Gamma_r), \quad (11)$$

with $\gamma_1 = -\partial_T \gamma(T, \Gamma)$, $\gamma_2 = -\partial_\Gamma \gamma(T, \Gamma)$. γ_0, T_r, Γ_r are reference values, whereas $\gamma(T, \Gamma)$ and γ_1 are experimentally known [46]. We note that the right-hand side (RHS) term $\partial_x \gamma(T, \Gamma)$ of Eqs. (9) is written in the literature [32,52] as $\epsilon \partial_x^2 \xi$ for isothermal condition. Demonstrating their equality uses the diffusion equation of adsorbed insoluble molecules (nematogens) at the interface, owing to their mobility. The

dynamics of molecule concentration satisfies the linearized equation about the equilibrium state Γ_0 [45,54,55]:

$$\partial_t \Gamma + \Gamma_0(\partial_x v_x) = D\partial_x^2 \Gamma. \quad (12)$$

The first term on the left-hand side (LHS) of the above equation is for the temporal change rate of concentration. The second term is the advected flux due to the interfacial flux of molecules. The term on the RHS is the diffusion of molecules with single-particle diffusion coefficient D , whose value is usually minimal. From the discussion above $\gamma_2 = -\partial\gamma/\partial\Gamma$, and by taking partial derivation ∂_x of Eq. (11) yields $\partial_x \gamma = -\gamma_1 \partial_x T - (\epsilon/\Gamma_0)\partial_x \Gamma$. Approximating $D \approx 0$, the diffusion equation reduces with the kinematic condition $\partial_t \xi = v_x$ at $z = 0$ to $\partial_t[\Gamma + \Gamma_0 \partial_x \xi] = 0$. Its solution is $\Gamma + \Gamma_0 \partial_x \xi = \text{const}$. By getting Γ , its x derivative yields $\partial_x \Gamma = -\Gamma_0 \partial_x^2 \xi$, from which it results $\partial_x \gamma = -\gamma_1 \partial_x T + \epsilon \partial_x^2 \xi$. Solutions to Eq. (3) consider a Dirichlet boundary condition of a thermally insulated interface $\partial_z T = 0$ at $z = 0$ [42,43]. In the rest of the paper, we will use Eqs. (1)–(11) to calculate the Faraday instability in the NLC with a free surface exposed to air and under an external acceleration while the interface experiences a temperature gradient. In their experiments, Roh *et al.* [25] considered the interfacial mobility of a flowing aqueous solution of insoluble surfactants on a NLC. Such a system consists of solvent water with dispersed solute surfactants. A given concentration of surfactant adsorbs to the interface with an NLC. A flow parallel to the interface acts on the surfactant solution side. In the absence of flow, an appropriate model to account for the interfacial elasticity of the insoluble solute surfactants adsorbed at the interface with the NLC was proposed by Rey [28,32]. Neglecting interface bending modes, according to Refs. [32,52], the generalization of the zz , xy components of the boundary conditions for σ^r become

$$\begin{aligned} \sigma_{zz}^r &= f_z^s = [\gamma(T, \Gamma) + W]\partial_x^2 \zeta(x) + \lambda \partial_x^3 \xi(x), \\ \sigma_{xz}^r &= f_x^s = -\lambda \partial_x^3 \zeta + \partial_x \gamma(T, \Gamma). \end{aligned} \quad (13)$$

Here, W is the anchoring energy of the NLC. λ represents the magnitude of coupling of in-plane deformation ξ of the interface with the perpendicular deformation ζ . In what follows, we provide the dispersion relations of the generated parametric instability, including this generalized form of the stresses. However, the numerical results presented below in Sec. V for the Faraday wave do not include W and λ .

A. Solution of hydrodynamic equations

In this section, we solve the Navier-Stokes Eq. (2) with the help of the boundary conditions for the perpendicular velocity component v_z to the interface. Because of its time variation, it relates to the interface height profile deformation ζ . The applied time-dependent vertical forcing $g(t)$ on the fluid allows a Floquet expansion of the velocity in terms of temporal modes, which leads to a recurrence relation for the interface deformation $\zeta(t)$. It is easiest to solve Eqs. (1)–(12) by using a Fourier transformation of each space-dependent function of the form $\mathcal{F}(f(x, z, t)) = \int dx e^{-ikx} f(x, z, t) = \tilde{f}(k, z, t)$, $i = \sqrt{-1}$, with the property $\mathcal{F}(\partial_x^m f(x, z, t)) = (ik)^m \tilde{f}(k, z, t)$ in the case of wave vector \mathbf{k} along the x axis. From the boundary condition at the interface $z = 0$, the shear stress must satisfy

the balance equation $\sigma_{xz} = 0$ which together with Eqs. (13) for σ_{zz}^r , and that of σ_{xz}^r , all transformed to Fourier space, yields a relationship for the velocity component \tilde{v}_z as

$$(\partial_z^2 - k^2)\partial_t \tilde{v}_z = \nu_1(\partial_z^2 - k^2)(\partial_z^2 - k^2)\tilde{v}_z - \nu' k^2 \partial_z^2 \tilde{v}_z, \quad (14)$$

where $\nu' = \eta'/\rho$, $\nu_1 = \eta_1/\rho$ and $\nu_2 = \eta_2/\rho$ are the kinetic viscosities.

Since the forcing $g(t)$ is a periodic function with period $2\pi/\omega$, we can use a Floquet expansion of space- and time-dependent functions of the type [48]

$$\tilde{f}(k, z, t) = \sum_{n=-\infty}^{\infty} \tilde{f}_n(k, z) e^{\mu_n t}, \quad (15)$$

with $\mu_n = s + i(n + \beta)\omega$, s and β being real valued. This representation allows obtaining the harmonic solutions (Hr) of Eq. (14) with $\beta = 0$ and subharmonic ones (Sh) with $\beta = 1/2$. Since \tilde{f} are real valued, then $\tilde{f}_n^* = \tilde{f}_{-n}$ for Hr and the relation holds $\tilde{f}_{n-1}^* = \tilde{f}_{-n}$ for Sh, where $*$ means complex conjugate.

Using the Floquet expansion in Eq. (14), we arrive at the ordinary differential equation for the velocity modes \tilde{v}_{zn} ,

$$\{\partial_z^4 + b_n \partial_z^2 + c_n\} \tilde{v}_{zn} = 0, \quad (16)$$

where

$$b_n = -\left[\frac{\mu_n}{\nu_1} + k^2\left(2 + \frac{\nu'}{\nu_1}\right)\right] \quad \text{and} \quad c_n = k^2\left[k^2 + \frac{\mu_n}{\nu_1}\right]. \quad (17)$$

The solution of Eq. (16) is

$$\begin{aligned} \tilde{v}_{zn} &= A_n \cosh z \sqrt{m_1} + B_n \sinh z \sqrt{m_1} \\ &\quad + C_n \cosh z \sqrt{m_2} + D_n \sinh z \sqrt{m_2}, \end{aligned} \quad (18)$$

where $m_1 = m_+$ and $m_2 = m_-$ are the two solutions of the quadratic equation $m^2 + b_n m + c_n = 0$. The unknown constants A_n, B_n, C_n , and D_n are determined below from Eqs. (1)–(6), including Eqs. (10) and (12). First, the solution of Eq. (3) for the temperature is also expressed in terms of Floquet components:

$$\tilde{\Gamma}_n = \frac{\Gamma_0 \partial_z \tilde{v}_{zn}}{\mu_n + k^2 \mathcal{D}}. \quad (19)$$

Note that the Floquet expansion of Eq. (15) permits the solution of Eq. (3) of the temperature

$$\{\partial_z^2 - a_n^2\} \tilde{T}_n = -\frac{A}{\alpha} \tilde{v}_{zn}, \quad (20)$$

where $a_n = \sqrt{k^2 + \mu_n/\alpha}$. Further, we eliminate v_x in the second of Eqs. (13) by taking $\partial_x \sigma_{xz} = \partial_x f_x^{(s)}$ after which, using a Fourier transformation and Floquet expansion, results in the new boundary condition at $z = 0$:

$$-\eta_1(\partial_z^2 + k^2)\tilde{v}_{zn} = -\lambda k^4 \tilde{\zeta}_n - \gamma_1 k^2 [A \tilde{\zeta}_n - \tilde{T}_n] + \gamma_2 k^2 \tilde{\Gamma}_n. \quad (21)$$

On the other hand, the pressure p at $z = 0$ is $-p + \rho g(t)\zeta + 2\eta_2 \partial_z v_z = [\gamma(T, \Gamma) + W]\partial_x^2 \zeta + \lambda \partial_x^3 \xi$. From Eq. (2), it is calculated $\rho \partial_t \partial_x \hat{\mathbf{e}}_x \cdot \mathbf{v} = \nabla \partial_x \hat{\mathbf{e}}_x \cdot \sigma$, in which we substitute p .

A Fourier-Floquet transformation leads to the new boundary condition at $z = 0$,

$$\{(\mu_n + 3\nu_1 k^2 + \nu' k^2)\partial_z - \nu_1 \partial_z^3\} \widetilde{v}_{z_n} + k\omega_0^2 \widetilde{\zeta}_n + \frac{\lambda}{\rho} i k^5 \widetilde{\xi}_n = \frac{ak^2}{2} (\widetilde{\zeta}_{n+1} + \widetilde{\zeta}_{n-1}), \quad (22)$$

with $\omega_0^2 = gk + [\gamma(T, \Gamma) + W]k^3/\rho$. Notice that the Euler formula for $\cos(\omega t)$ yields $\widetilde{\zeta}_{n+1} = \widetilde{\zeta}_n e^{i\omega t}$, $\widetilde{\zeta}_{n-1} = \widetilde{\zeta}_n e^{-i\omega t}$.

Finally, the four unknown constants A_n, \dots, D_n are derived from the four Eqs. (5), (6), (20), and (21). After that, the determined A_n, \dots, D_n are replaced in Eq. (22), which is satisfied by \widetilde{v}_{z_n} yielding the recurrence relation for ζ_n ,

$$\mathbb{D}_n \widetilde{\zeta}_n = a(\widetilde{\zeta}_{n+1} + \widetilde{\zeta}_{n-1}), \quad (23)$$

with

$$\begin{aligned} \frac{k}{2} \mathbb{D}_n(k, \mu_n) = & \omega_0^2 + \frac{1}{k\mu_n} \{ \sqrt{c_n} [\Phi_n r_n + \Theta_n s_n - (\Phi_n s_n + \Theta_n r_n) \cosh L \sqrt{m_1} \cosh L \sqrt{m_2}] \\ & + (\Phi_n s_n m_2 + \Theta_n r_n m_1) \sinh L \sqrt{m_1} \sinh L \sqrt{m_2} + \sqrt{c_n} \mu_n p_n [s_n \cosh L \sqrt{m_2} - r_n \cosh L \sqrt{m_1}] \\ & + \sqrt{c_n} m_1 \mu_n k^2 (m_1 - m_2) [R_n q_n + (Q_n + b_n q_n) \mu_n \nu_1] \sinh L \sqrt{m_1} \cosh L \sqrt{m_2} \\ & + k^2 \mu_n [\sqrt{c_n} m_2 s_n (Q_n + q_n m_2) - \sqrt{m_1} r_n (q_n c_n + Q_n m_2)] \cosh L \sqrt{m_1} \sinh L \sqrt{m_2} / \\ & \{ P_n [\sqrt{m_1} \cosh L \sqrt{m_1} \sinh L \sqrt{m_2} - \sqrt{m_2} \cosh L \sqrt{m_2} \sinh L \sqrt{m_1}] \\ & + k^2 \sqrt{c_n} (b_n q_n - 2Q_n) [\cosh L \sqrt{m_1} \cosh L \sqrt{m_2} - 1] + k^2 (2c_n q_n - b_n Q_n) \sinh L \sqrt{m_1} \sinh L \sqrt{m_2} \\ & + p_n [\sqrt{m_2} \sinh L \sqrt{m_1} - \sqrt{m_1} \sinh L \sqrt{m_2}] \}. \end{aligned} \quad (24)$$

Other quantities appearing in Eq. (24) are defined in the Supplemental Material [56]. Equation (24) depends on the Marangoni number of temperature gradient $M_T = \gamma_1 l_c^2 A / (\eta_1 \alpha)$, and the particles' concentration gradient $M_\Gamma = \gamma_2 \Gamma_0 l_c / (\eta_1 \mathcal{D})$, with l_c a system characteristic length scale. The semi-infinite limit $L \rightarrow \infty$ of Eq. (24) for a NLC corresponds to $\text{sech}(La_n) \rightarrow 0$ and $\tanh(La_n) \rightarrow 1$, thus

$$\begin{aligned} \frac{k}{2} \mathbb{D}_n^{(\infty)}(k, \mu_n) = & \omega_0^2 + \frac{1}{k\mu_n} \left\{ -\Phi_n s_n (\sqrt{c_n} - m_2) - \Theta_n r_n (\sqrt{c_n} - m_1) + \sqrt{c_n} m_1 \mu_n k^2 (m_1 - m_2) \left[R_n \frac{A\gamma_1}{\alpha\rho} + \left(Q_n + b_n \frac{A\gamma_1}{\alpha\rho} \right) \mu_n \nu_1 \right] \right. \\ & \left. + \mu_n k^2 \left[\sqrt{c_n} m_2 s_n \left(Q_n + \frac{A\gamma_1}{\alpha\rho} m_2 \right) - \sqrt{m_1} r_n \left(c_n \frac{A\gamma_1}{\alpha\rho} + Q_n m_2 \right) \right] \right\} / \left\{ P_n (\sqrt{m_1} - \sqrt{m_2}) \right. \\ & \left. + k^2 \left[\frac{A\gamma_1}{\alpha\rho} (\sqrt{c_n} b_n + 2c_n) - (2\sqrt{c_n} + b_n) Q_n \right] \right\}. \end{aligned} \quad (25)$$

III. APPLIED MAGNETIC FIELD PARALLEL TO THE WAVE VECTOR ORIENTED ALONG THE y AXIS. NEMATIC DIRECTOR PARALLEL TO THE INTERFACE

In this case, the nematic director is in the direction $\mathbf{n} = \hat{\mathbf{e}}_y$, and the magnetic field is parallel to the director. The balance equation $\sigma_{yz} = 0$ implies that the director is perpendicular both to the velocity field $\mathbf{v} = v_x \hat{\mathbf{e}}_x + v_z \hat{\mathbf{e}}_z$ and the wave vector $k\hat{\mathbf{e}}_y$. Therefore, there is no coupling between the director and the velocity, and the hydrodynamic equations for the free interface are the same as that of a Newtonian liquid with one viscosity $\eta = \eta_1 = \eta_2$, $\nu = \eta/\rho$. In this case, Eqs. (24) and (25) do not change; however, now $\nu' = 0$ and therefore $b_n = -2k^2 - \mu_n/\nu$. In this way, the solution to Eq. (16) has the two roots: $m_1 = k^2 + \mu_n/\nu$ and $m_2 = k^2$.

IV. MAGNETIC FIELD PARALLEL TO z AXIS. NEMATIC DIRECTOR PERPENDICULAR TO THE INTERFACE

Now the nematic director is $\mathbf{n} = \hat{\mathbf{e}}_z$. $z = \zeta(x, t)$ [46]. Therefore, there is symmetry in the plane xy . Thus, from Eq. (1), $\sigma'_{xz} = \eta_1 (\partial_z v_x + \partial_x v_z) = 0$ and $\sigma'_{yz} = \eta_1 (\partial_z v_y + \partial_y v_z) = 0$. However, the condition $\sigma_{zx} = 0$ leads to $v_y = 0$ again. Thus, following the same procedure as in Sec. I,

two oscillation modes appear to fulfill the same characteristic Eq. (16) despite the boundary condition Eq. (13) being different from the ones in Secs. I and II above. In this case, the boundary condition is $-p + \rho g(t)\zeta + (\eta' + 4\eta_1 - 2\eta_2)\partial_z v_z = \gamma(T, \Gamma)\partial_z^2 \zeta + \lambda\partial_z^3 \xi$. Using these facts and performing the procedure described in Sec. I, the same recurrence relation of Eq. (23) results.

V. RESULTS

In this section, a numerical analysis of Eqs. (23) and (24) provide the values of the critical acceleration a_c and wave number k_c at the parametric instability onset. For the nematic liquid MBBA, all the material parameters are known experimentally [20,46,57]. Thus, Eqs. (23) and (24) do not contain unknown free parameters. It is interesting to research the effect of temperature gradient on the Faraday wave as accounted for by the Marangoni number $M_T = \gamma_1 l_c^2 A / (\eta_1 \alpha)$ [42,43]. A is the temperature gradient concerning the base state, namely, $A = -(T_{00} - 273.15)/L$, the temperature increment from liquid-air free surface towards the bottom. The critical acceleration and wave number are the minimum threshold values they acquire at the onset of the

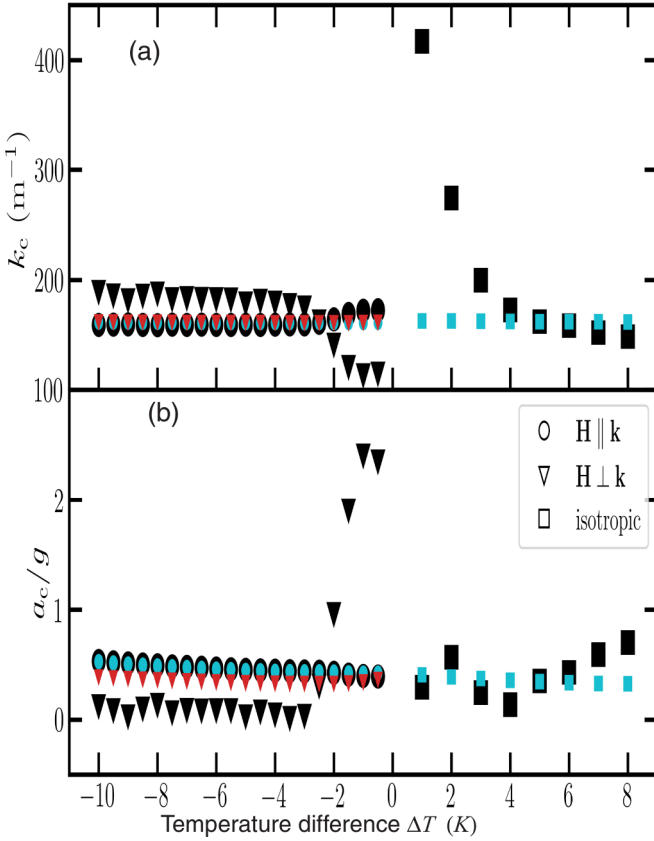


FIG. 1. Calculated critical parameters: k_c (a) and a_c (b) as a function of the MBBA nematic-isotropic transition temperature difference $\Delta T = T - T_c$ of a subharmonic wave. External frequency $\omega = 20\pi$ Hz circles symbol \circ with $\mathbf{H} \parallel \mathbf{k}$, triangle symbol ∇ for $\mathbf{H} \perp \mathbf{k}$ in the nematic phase. Layer thickness used $L = 0.0045$ m. The same properties k_c , a_c in the isotropic phase are depicted with square symbol \square . Filled-black symbols include Marangoni convection $M_T = \gamma_1 l_c^2 A / (\eta_1 \alpha)$ due to temperature gradient. Grey symbols (online red and blue cyan colors) do not include the Marangoni effect $M_T = 0$. Used material data of MBBA as cited in Ref. [18].

instability for given forcing $g(t)$. This $k_c = |\mathbf{k}|$ is the eigenvector magnitude obtained from Eq. (23) for an $n = 22$ number of nodes and parameter $s = 0$ [48]. To numerically determine k_c from Eq. (23), we used the material properties of MBBA as cited by Ref. [18]. These include the experimental values of the viscosities η_1 , η_2 , η' , the surface tension γ as a function of temperature [46,57] about the transition temperature from nematic to isotropic phase, namely, $T_c \approx 318$ K. There are also the thermal diffusivity values α from the experiments of Urbach *et al.* [20]. As a working hypothesis, the density of liquid crystal is constant: $\rho = 1.03881 \times 10^3$ Kg/m³. Figure 1 shows the plots of k_c , Fig. 1(a), and a_c , Fig. 1(b), as a function of temperature for frequency $\omega = 20\pi$ Hz and for a liquid layer thickness, $L = 0.0045$ m.

In this plot, all generated waves are of subharmonic types. Black-filled symbols represent solutions of Eqs. (23) and (24) with the effect of a temperature gradient, that is, $M_T \neq 0$. For comparison purposes, in this plot are also those values without temperature variation, $M_T = 0$ calculated from Eq. (3) of the Supplemental Material [56]. Their values are in red and cyan

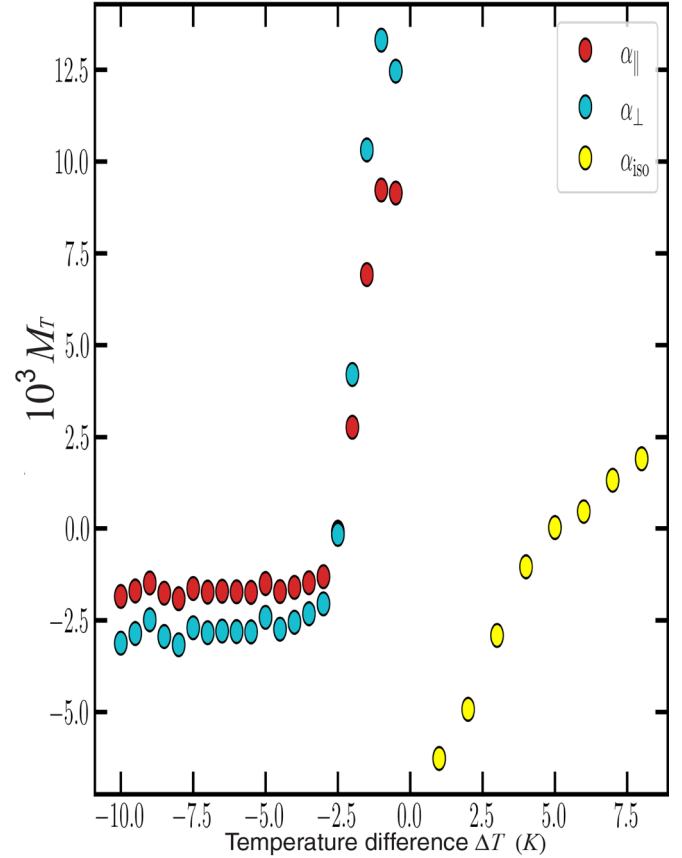


FIG. 2. The calculated Marangoni number $M_T = \gamma_1 l_c^2 A / (\eta_1 \alpha)$ versus temperature difference $\Delta T = T - T_c$ about the critical temperature $T_c = 388$ K for MMBA liquid crystal. In the nematic phase, the heat thermal diffusivity is anisotropic, being α_{\parallel} for its measurement along the optical molecular axis (filled-black circle symbol, red color online), α_{\perp} shadow (cyan color online), circle symbol. The nematic liquid with depth $L = 0.0045$ m. The isotropic case is for $\Delta T = T - T_c \geq 0$ K. $l_c = \sqrt{\gamma / \rho g}$ is the capillary length. The temperature gradient A values are tabulated in Supplemental Material [56]. Used data for α_{\parallel} , α_{\perp} of MBBA as cited in Ref. [18]. Note that α scale as 10^{-7} m²/s.

color-filled symbols. More specifically, circles represent when the magnetic field orients the nematic director in the direction parallel to the wave vector $\mathbf{H} \parallel \mathbf{k}$. Triangles represent a system where the magnetic field orients the director perpendicular to the wave vector $\mathbf{H} \perp \mathbf{k}$. In this last case, it is true that $\eta = \eta_1 = \eta_2$ and $\eta' = 0$. The liquid behaves as a simple isotropic Newtonian liquid with a single viscosity since the director is perpendicular to the local optic axis (see Sec. III). A different study in Ref. [18] assumed a constant temperature gradient A , which is different from the present paper, where it is a varying quantity. This fact resides in the experimental data that fixes a given temperature at the liquid-air interface. That is, in the experiments, at the bottom of the layer $T = 273$ K and varies up to the interface where it reaches the desired temperature $T_0 \neq 0$. According to Fig. 1, the effect of temperature gradient on the threshold values a_c is insignificant for the case $\mathbf{H} \parallel \mathbf{k}$. However, as the nematic-isotropic transition temperature is reached, namely, -2 K $< \Delta T = T - T_c < 0$ K, there is a

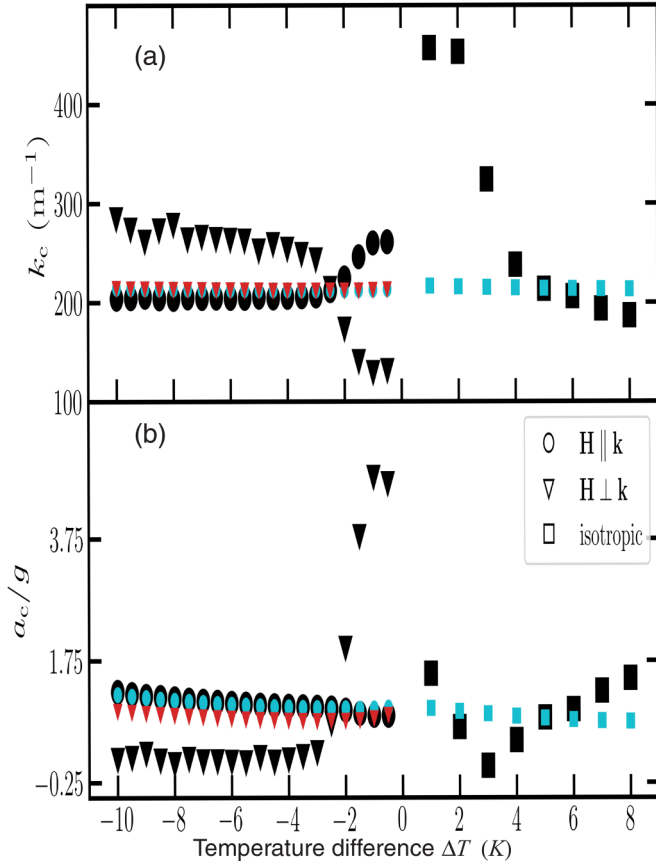


FIG. 3. Subharmonic's threshold wave number k_c (a) and acceleration a_c (b) versus temperature of MBBA nematic liquid with depth $L = 0.0025$ m and forcing frequency $\omega = 20\pi$ Hz. Black-filled symbols include Marangoni convection $M_T = \gamma_1 l_c^2 A / (\eta_1 \alpha)$ whereas shadow symbols without it (cyan and red color symbols online).

significant change in k_c for $T - T_c > 0$ K where there is a steep change of its magnitude of about 75% in this isotropic phase concerning its last value in the nematic phase.

However, the system with $\mathbf{H} \perp \mathbf{k}$ (symbol \blacktriangledown), Fig. 1(b), shows that when a temperature gradient is non-negligible, $M_T \neq 0$, the overall strength of a_c drops in the nematic phase $\Delta T = T - T_c < 0$ K in comparison to the case with $M_T = 0$. In contrast, the magnitudes of their corresponding wave numbers k_c are in the reverse order, respectively; see Fig. 1(a).

Approaching the critical temperature from the nematic phase, $-2 \text{ K} < \Delta T = T - T_c < 0 \text{ K}$, and case $M_T \neq 0$, k_c drops below its value when $M_T = 0$. In the same temperature range, the threshold acceleration a_c starts experiencing a sharp increase, reaching a maximum value of about $\Delta T = T - T_c \approx 1 \text{ K}$ for $M_T \neq 0$. After that, the temperature difference $\Delta T = T - T_c > 0 \text{ K}$ crosses towards the isotropic phase, where a_c oscillates and finally increases monotonously for higher temperatures $\Delta T = T - T_c \geq 4 \text{ K}$. Summarizing, when temperature gradients are absent, $M_T = 0$, both a_c (and k_c) of the instability wave show almost constant values from the nematic to the isotropic phase, with a slight decrease (increase) in its slope toward the isotropic phase and

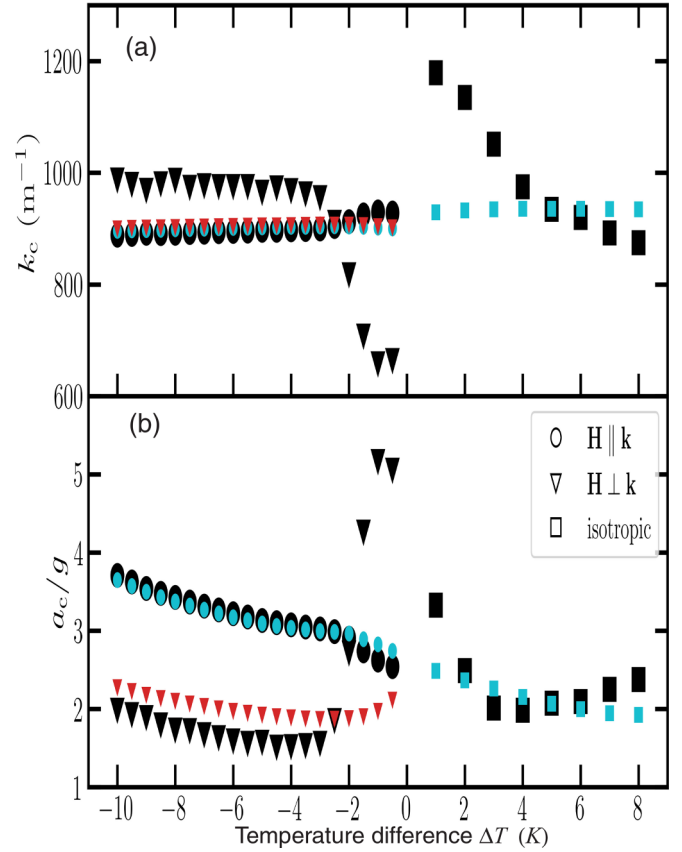


FIG. 4. Subharmonic's threshold wave number k_c (a) and acceleration a_c (b) versus temperature of MBBA nematic liquid with depth $L = 0.0045$ m and forcing frequency $\omega = 120\pi$ Hz. Black-filled symbols include Marangoni convection $M_T = \gamma_1 l_c^2 A / (\eta_1 \alpha)$ whereas shadow symbols without it (cyan and red color symbols online)—same materials parameters of Fig. 1.

further. Equation (24) does not explicitly contain the Marangoni number. $M_T = \gamma_1 l_c^2 A / (\eta_1 \alpha)$ [42,43]. This fact allows us to define the characteristic length l_c differently. One form is to define it as $l_c = \sqrt{(\gamma / \rho g)}$. Thus, $Al_c = -\Delta T^{(s)}$ represents the temperature change from the base state (bottom of the layer) up to height l_c towards the interface. Note that Urbach *et al.* [20] measures two thermal conductivity values α in the nematic phase: one for heat propagation along the molecular optical axis α_{\parallel} whereas another is perpendicular to it, α_{\perp} . Numerically, any of these two values of α are used in solving Eqs. (23) and (24), and they do not lead to any different results of the calculated acceleration $a_c(k_c, \omega)$, which is insensitive to the anisotropy of α . Similarly, the Marangoni number $M_T = \gamma_1 l_c^2 A / (\eta_1 \alpha)$ does not experience any change with either value of the anisotropic α as depicted in Fig. 2.

Figure 2 plots the calculated Marangoni number M_T as a function of the gradient in temperature difference $\Delta T = T - T_c$ across the nematic-isotropic phase transition of MBBA liquid crystal. Here l_c is the capillary length $\sqrt{(\gamma / \rho g)}$. We observed that the Marangoni number experiences a significant change in the nematic phase, where it goes from a -2.5×10^3 value in the range of temperatures $-10 \text{ K} < \Delta T = T - T_c < -2 \text{ K}$ and shows a step increase in $-2 \text{ K} < \Delta T = T - T_c$

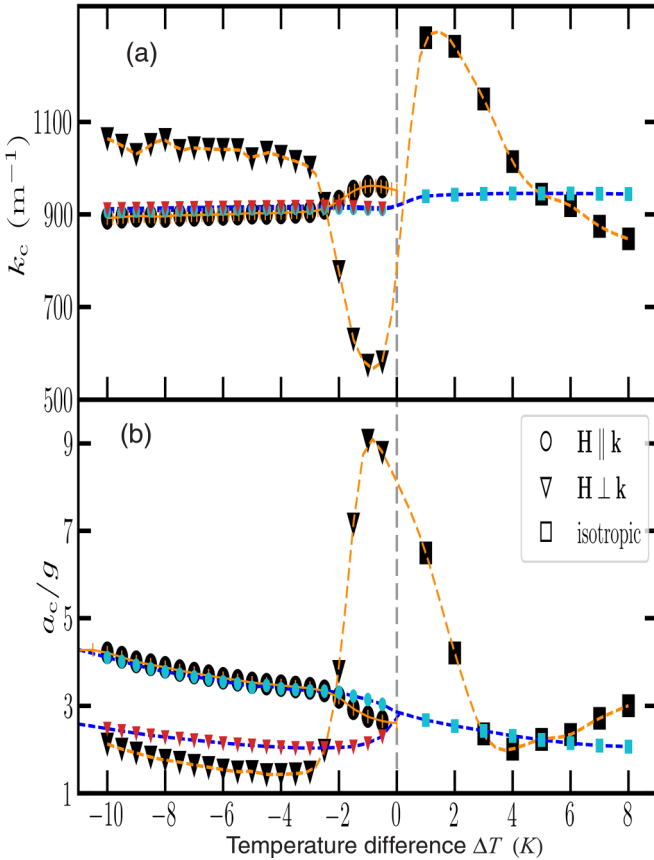


FIG. 5. Subharmonic's threshold wave number k_c (a) and acceleration a_c (b) versus temperature of MBBA nematic liquid with depth $L = 0.0025$ m and forcing frequency $\omega = 120\pi$ Hz. Black-filled symbols \bullet , \blacksquare , \blacktriangledown include Marangoni flow $M_T = \gamma_1 l_c^2 A / (\eta_1 \alpha)$ whereas shadow symbol without it (cyan and red color symbols online). Dashed lines are guides to the eyes—the same material parameters as Fig. 1.

< 0 K. After the critical transition temperature, M_T drops to -6×10^3 and increases monotonously in the isotropic phase as the temperature increases.

Figure 3 shows the critical wave number k_c , Fig. 3(a), and acceleration a_c , Fig. 3(b), of excited Faraday instability. The nematic layer of depth $L = 0.0025$ m is almost half the size used in Fig. 1. The forcing frequency is $\omega = 20\pi$ Hz, and the use of the same material parameters as in Fig. 1 for the nematic MBBA. Reducing to half the layer thickness from $L = 0.0045$ m, Fig. 1, to $L = 0.0025$ m has the effect of increasing the strength of the threshold values of k_c, a_c , as seen in Fig. 3 versus Fig. 1. Also, their values near the critical temperature are more pronounced than in Fig. 1 of a thicker layer. There is still continuous evolution on these dynamical parameters from the nematic to isotropic phase remaining almost constant for $M_T = 0$ and case of $\mathbf{H} \parallel \mathbf{k}$. Nonetheless, in the case $M_T \neq 0$ that includes temperature gradient, and with the condition $\mathbf{H} \perp \mathbf{k}$, the parameters k_c, a_c show sharp changes in the phase transition.

Figures 4 and 5 depict the effect of a higher frequency $\omega = 120\pi$ Hz on the Faraday instability critical wave number and acceleration as a function of temperature for a thicker layer

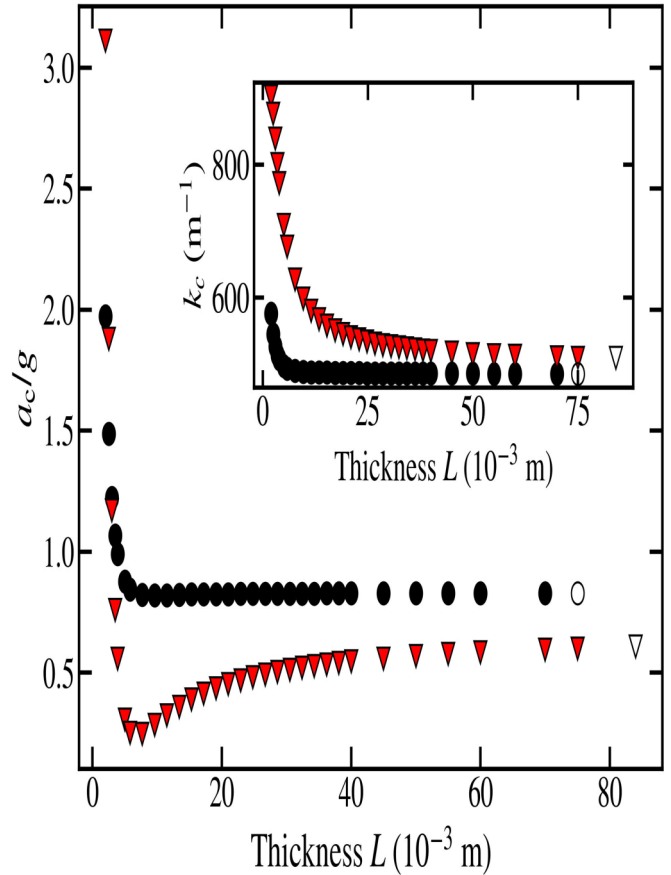


FIG. 6. Subharmonic acceleration a_c versus liquid layer thickness L at forcing frequency $\omega = 60\pi$ Hz while taking into account the temperature gradient given by the Marangoni number $M_T = \gamma_1 l_c^2 A / (\eta_1 \alpha)$. Symbol \bullet is for MBBA nematic liquid at $\Delta T = T - T_c = -2$ K, whereas the red-filled triangle corresponds to isotropic phase at $\Delta T = T - T_c = 2$ K. In the same plot, symbols \circ and ∇ results from a semi-infinite layer $L \rightarrow \infty$. Inset depicts threshold wave number k_c versus L .

than in Figs. 1 and 3, and a layer of thickness $L = 0.0045$ m for Fig. 4 and $L = 0.0045$ m for Fig. 5.

The material parameters of MBBA liquid crystal are the same as in Fig 1. Increasing the excitation frequency ω increases the magnitudes of a_c, k_c concerning their values for $\omega = 20\pi$ Hz. However, we notice a notorious difference in the values of a_c, k_c between the cases $\mathbf{H} \parallel \mathbf{k}$ and $\mathbf{H} \perp \mathbf{k}$ when there is Marangoni flow $M_T \neq 0$. In the latter case, k_c becomes nonmonotonous and discontinuous at the critical temperature with a high value after $T_c = 388$ K, whereas a_c increases steeply about $\Delta T = T - T_c \approx 1$ K in the nematic phase, then following a minimum in the Isotropic phase and increasing for higher temperatures. Figure 5 shows that the discontinuity in the values of a_c, k_c is more critical for reduced layer size and more significant frequencies than Figs. 1 and 3.

Figure 6 depicts the critical acceleration of subharmonic waves as a function of average liquid layer thickness L for the forcing frequency $\omega = 60\pi$ Hz. In this case, advected Marangoni flow is present due to temperature gradient at $T - T_c = -2$ K in the nematic phase of MBBA liquid crystal (symbol \bullet). In the isotropic phase at $\Delta T = T - T_c = 2$ K, the

same property is plotted with the symbol red-filled triangle. The same properties are calculated in the limit of the semi-infinite layer $L \rightarrow \infty$. The results are in \circ and ∇ symbols. As a summary of Figs. 1–6, the linear hydrodynamic theory Eq. (21) can capture the differences between the unstable surface wave generated on a nematic's surface and the isotropic phase of the liquid crystal.

VI. CONCLUSION

We demonstrated that a hydrodynamic description of Faraday instability in nematic liquid crystalline fluids is possible, Eqs. (23) and (24). This fact is confirmed through Fig. 1, where the threshold critical wave number k_c and acceleration a_c at instability onset were calculated using known material

parameters of MBBA nematic liquid and without free parameters in Eq. (24). These observables are amenable to being measured experimentally. We have shown in Fig. 1 that due to the temperature gradient, the Marangoni flow drives a more significant change in the threshold values of k_c and a_c close to the critical isotropic-nematic phase transition temperature than when it is not present. Its effect is more critical when the magnetic field orients the nematogen molecules of the liquid in a perpendicular direction than parallel to the wave vector. Interestingly, the Marangoni number of temperature gradient also shows a considerable variation near the isotropic-nematic phase transition temperature, see Fig. 2. Reducing the liquid layer thickness or increasing the shaker forcing frequency still emphasized these abrupt changes on k_c and a_c at the phase transition temperature, as can be seen in Figs. 3–6.

-
- [1] W. S. Edwards and S. Fauve, *J. Fluid Mech.* **278**, 123 (1994).
 - [2] S. Douady, *J. Fluid Mech.* **221**, 383 (1990).
 - [3] K. Kumar, *Proc. R. Soc. Lond. A* **452**, 1113 (1996).
 - [4] H. W. Müller, H. Wittmer, C. Wagner, J. Albers, and K. Knorr, *Phys. Rev. Lett.* **78**, 2357 (1997).
 - [5] H. W. Müller, *Phys. Rev. Lett.* **71**, 3287 (1993).
 - [6] V. V. Mekhonoshin and A. Lange, *Phys. Rev. E* **65**, 061509 (2002).
 - [7] T. Mahr and I. Rehberg, *Phys. Rev. Lett.* **81**, 89 (1998).
 - [8] H. W. Müller and W. Zimmermann, *Europhys. Lett.* **45**, 169 (1999).
 - [9] C. Wagner, H. W. Müller, and K. Knorr, *Phys. Rev. Lett.* **83**, 308 (1999).
 - [10] F. Raynal, S. Kumar, and S. Fauve, *Eur. Phys. J. B* **9**, 175 (1999).
 - [11] S. Kumar, *Phys. Fluids* **11**, 1970 (1999).
 - [12] P. Huber, V. P. Soprunyuk, J. P. Embs, C. Wagner, M. Deutsch, and S. Kumar, *Phys. Rev. Lett.* **94**, 184504 (2005).
 - [13] P. Ballesta and S. Manneville, *Phys. Rev. E* **71**, 026308 (2005).
 - [14] T. Epstein and R. D. Deegan, *Phys. Rev. E* **81**, 066310 (2010).
 - [15] P. Ballesta, M. P. Lettinga, and S. Manneville, *Soft Matter* **7**, 11440 (2011).
 - [16] P. Chen, Z. Luo, S. Guven, S. Tacoglu, A. Wneg, A. V. Ganesan, and U. Demirci, *Adv. Mater.* **26**, 5936 (2014).
 - [17] M. Hernández-Contreras, *J. Phys.: Condens. Matter* **22**, 035106 (2010).
 - [18] M. Hernández-Contreras, *Phys. Rev. E* **88**, 062311 (2013).
 - [19] R. Sarma and P. K. Mondal, *Phys. Rev. E* **97**, 043105 (2018).
 - [20] W. Urbach, H. Hervet, and F. Rondelez, *Mol. Cryst. Liq. Cryst.* **46**, 209 (1978).
 - [21] L. Thomas, W. Pesch, and G. Ahlers, *Phys. Rev. E* **58**, 5885 (1998).
 - [22] R. S. Akopayan, R. B. Alaverdyan, L. Kh. Muradyan G. E. Seferyan, and Yu. S. Chilingaryan, *Quantum Electron.* **33**, 81 (2003).
 - [23] H. Choi and H. Takezoe, *Soft Matter* **12**, 481 (2016).
 - [24] S. H. Shvetsov, A. S. Zolot'ko, G. A. Voronin, A. V. Emelyanenko, M. M. Avdeev, M. A. Bugakov, P. A. Statsenko, and S. I. Trashkeev, *Opt. Mater. Express* **11**, 1705 (2021).
 - [25] S. Roh, M. Tsuei, and L. Abbott, *Langmuir* **37**, 5810 (2021).
 - [26] J. Yoshioka, T. Sakikawa, Y. Ito, and K. Fukao, *Phys. Rev. E* **105**, L012701 (2022).
 - [27] I. K. Kitamura, K. Oishi, M. Hara, S. Nagano, and T. Seki, *Sci. Rep.* **9**, 2556 (2019).
 - [28] A. D. Rey, *J. Chem. Phys.* **110**, 9769 (1999).
 - [29] A. D. Rey, *Phys. Rev. E* **60**, 1077 (1999).
 - [30] A. D. Rey, *Langmuir* **22**, 219 (2006).
 - [31] J. B. Poursamad, *Optik* **127**, 4872 (2016).
 - [32] S. V. Lishchuk, *Phys. Rev. E* **76**, 011711 (2007).
 - [33] V. Popa-Nita and P. Oswald, *J. Chem. Phys.* **127**, 104702 (2007).
 - [34] G. Germano and F. Schmid, *J. Chem. Phys.* **123**, 214703 (2005).
 - [35] J. B. Poursamad, F. B. Jahanbakhsh, M. Asadpour, and A. Phirouznia, *J. Mol. Liq.* **186**, 23 (2013).
 - [36] J. B. Poursamad, M. Asadpour, A. Phirouznia, and M. Sahrai, *Optik* **125**, 997 (2014).
 - [37] H. N. W. Lekkerkerker, *J. Phys. Colloques* **40**, C3-67 (1979).
 - [38] Q. Feng, W. Decker, W. Pesch, and L. Kramer, *J. Phys. II France* **2**, 1303 (1992).
 - [39] P. J. Barratt and D. Sloan, *J. Fluid Mech.* **102**, 389 (1981).
 - [40] M. Velarde and I. Zuñiga, *J. Phys. France* **40**, 725 (1979).
 - [41] L. Kramer and W. Pesch, in *Pattern Formation in Liquid Crystals*, edited by M. Buka, L. Kramer (Springer, New York, 1996), pp. 221-255
 - [42] R. V. Birikh, V. A. Briskman, A. A. Cherepanov, and M. G. Velarde, *J. Colloid Interface Sci.* **238**, 16 (2001).
 - [43] M. A. Vila, V. A. Kuz, A. N. Garazo, and A. E. Rodriguez, *J. Phys. France* **48**, 1895 (1987).
 - [44] W. Urbach, F. Rondelez, P. Pieranski, and F. Rothen, *J. Phys. France* **38**, 1275 (1977).
 - [45] A. B. Mikishev, B. A. Friedman, and A. A. Nepomnyashchy, *Fluid Dyn. Res.* **48**, 061403 (2016).
 - [46] D. Langevin and M. A. Bouchiat, *J. Phys. France* **33**, 101 (1972).
 - [47] D. Langevin, *Scattering by Liquid Surfaces and Complementary Techniques* (Dekker, New York, 1992).
 - [48] K. Kumar and L. S. Tuckerman, *J. Fluid Mech.* **279**, 49 (1994).
 - [49] S. Fauve, K. Kumar, C. Laroche, D. Beysens, and Y. Garrabos, *Phys. Rev. Lett.* **68**, 3160 (1992).

- [50] N. Périnet, D. Juric, and L. S. Tuckerman, *J. Fluid Mech.* **635**, 1 (2009).
- [51] J. Giermanska-Kahn, F. Monroy, and D. Langevin, *Phys. Rev. E* **60**, 7163 (1999).
- [52] M. A. Buzza, J. L. Jones, T. C. B. McLeish, and R. W. Richards, *J. Chem. Phys.* **109**, 5008 (1998).
- [53] D. Langevin and M. A. Bouchiat, *Mol. Cryst. Liq. Cryst.* **22**, 317 (1973).
- [54] H. Wong, D. S. Rumschitzki, and C. Maldarelli, *Phys. Fluids* **8**, 3203 (1996).
- [55] M. G. Blyth and C. Pozrikidis, *Theor. Comput. Fluid Dyn.* **17**, 147 (2004).
- [56] See Supplemental Material at <http://link.aps.org/supplemental/10.1103/PhysRevE.108.054703> for Eq. (23) coefficients and its limits, and Table I of the gradient of temperature A .
- [57] D. Langevin, *J. Phys. France* **33**, 249 (1972).